Anomalous Behavior of Viscosity and Electrical Conductivity of $MgSiO_3$ melt at Mantle Conditions

Haiyang Luo[1]*, Bijaya B. Karki[1,2]*, Dipta B. Ghosh[1,2], Huiming Bao[1]

[1]Department of Geology & Geophysics, Louisiana State University, Baton Rouge, LA 70803, USA

[2]School of Electrical Engineering and Computer Science, Louisiana State University

Corresponding author: Haiyang Luo (hluo5@lsu.edu) ; Bijaya B. Karki (bbkarki@lsu.edu)

Key Points:

- The viscosity of $MgSiO_3$ melt behaves anomalously at relatively low temperatures; first decreasing and then increasing with pressure.
- The electrical (ionic) conductivity shows anomalous pressure behavior at all temperatures.
- Deep potential molecular dynamics simulations offer us a reliable and complete dataset to study transport properties of silicate melts.

Abstract

Silicate melts have served as transport agents in the chemical and thermal evolution of Earth. Molecular dynamics simulations based on a deep neural network potential trained by *ab initio* data show that the viscosity of $MgSiO_3$ melt decreases with increasing pressure at low pressures (up to ~6 GPa) before it starts to increase with further compression. The melt electrical conductivity also behaves anomalously; first increasing and then decreasing with pressure. The melt accumulation implied by the viscosity turnover at ~23 GPa along mantle liquidus offers an explanation for the low-velocity zone at the 660-km discontinuity. The increase in electrical conductivity up to ~50 GPa may contribute to the steep rise of Earth's electrical conductivity profiles derived from magnetotelluric observations. Our results also suggest that small fraction of melts could give rise to detectable bulk conductivity in deeper parts of the mantle.

Plain Language Summary

Dynamical behavior of silicate melts at high temperature and pressure controls melt distribution in Earth's interior. However, the experimental data on viscosity and electrical conductivity of silicate melts are limited to relatively low pressure. Moreover, the pressure dependence of viscosity is in debate, especially for depolymerized silicate melts. Using a new deep learning-based simulation approach, we find that both the viscosity and electrical conductivity of $MgSiO_3$ melt behave anomalously with pressure, which could have important implications for zones with seismic velocity anomalies and high electrical conductivity in Earth's interior.

1 Introduction

Silicate melts have been playing a critical role in the physico-chemical differentiation and evolution of Earth. During Earth's accretion, energy from multiple impact events and decay of radioactive isotopes likely led to a partially or completely molten early Earth (Canup, 2004). The viscosity of silicate melts controlled the dynamics of the early magma oceans and subsequently influenced petrologic and geodynamic processes, such as crystal settling and core-mantle differentiation (Elkins-Tanton, 2012; Solomatova, 2007). The mobility of magma in the present-day Earth is also governed by melt viscosity, in addition to melt-solid density contrast (Schubert et al., 2001). Many variables influence melt viscosity, including temperature, pressure, and composition (Ni et al., 2015). Yet contrasting conclusions have been inferred from experiments on the pressure dependence of viscosity, especially for depolymerized silicate melts (Cochain et al., 2017; Liebske et al., 2005; Reid et al., 2003; Spice et al., 2015). Early studies on molten diopside ($CaMgSi_2O_6$) and peridotite showed an initial increase in viscosity with pressure, followed by a decrease above ~10 GPa (Liebske et al., 2005; Reid et al., 2003). Later studies on molten fayalite (Fe_2SiO_4) and end-member pyroxenite melts ($MgSiO_3$ and $CaSiO_3$) reported a decrease in viscosity with pressure up to ~8 GPa (Cochain et al., 2017; Spice et al., 2015). In addition, these investigated viscosities of silicate melts by experiments have been limited to relatively low pressure (<13 GPa) except one recent study that has extended the pressure up to 30 GPa (Xie et al., 2020). The electrical conductivity of silicate melts is another fundamental property needed to interpret the variations of electrical conductivity and explore the composition and structure of Earth's interior. But, it remains unknown over almost the entire mantle pressure regime (up to ~136 GPa) (Ni et al., 2015).

First-principles computation is a powerful complementary approach, which has been widely used in the study of silicate melts. However, computational studies of transport properties

of silicate melts have been typically limited to relatively high temperatures (≥3000 K) due to high computational costs (e.g., Ghosh & Karki, 2017; Karki & Stixrude, 2010; Verma & Karki, 2012). Moreover, these calculated results are considerably scattered in pressure-temperature space. A recently developed deep-learning method has been demonstrated to be orders of magnitude faster than the first-principles approach with comparable *ab initio* accuracy (e.g., Wang et al., 2018; Zhang et al., 2018a). A well-trained deep-learning potential can greatly enhance sampling and offer us a reliable and complete dataset to study the viscosity and electrical conductivity of silicate melts under pressure and temperature conditions that are directly relevant to the mantle regime. Here, we investigate the viscosity and electrical conductivity of $MgSiO_3$ melt at Earth's mantle conditions using the deep-learning potential method.

2 Materials and Methods

We constructed the deep-learning potential (DP) model for $MgSiO_3$ melt using the DP-GEN (Zhang et al., 2020) scheme for the configurational space covering a temperature range 2200-5000 K and a volume range $0.5V_x$-$1.2V_x$, where V_x = 38.9 cm^3/mol is the experimental volume at the ambient melting point of 1830 K (Lange & Carmichael, 1987). The DP-GEN scheme works iteratively, and each iteration includes three stages: exploration, labeling, and training. To begin with, rough DP models are first trained by a simple data set. Then, DP-GEN starts to explore the configurational space by DP-based molecular dynamics simulations. The explored configurations are categorized as failed, candidate, and accurate, according to the maximum deviation of forces ($\delta_f^{\max}$), defined as $\delta_f^{\max} = \max_i \sqrt{\langle \|f_i - \langle f_i \rangle\|^2 \rangle}$, where f_i is the force acting on atom i, and $\langle \dots \rangle$ represents the average of the DP model ensemble. The failed and accurate sets include configurations with large force deviations ($\delta_f^{max} > \delta_{high}$) and small force deviations ($\delta_f^{\max} < \delta_{\mathrm{low}}$), respectively, where δ_{high} and δ_{low} are user-provided. The configurations with maximum force deviations between δ_{low} and $\delta_{\mathrm{high}}$are classified as candidates, a subset of which is then labeled with energy and force by high-precision DFT calculations and added to the existing data set for the next training. A new exploration stage begins by using the newly trained DP models based on the updated data set. A good convergence of the DP-GEN iterations is achieved when almost all the explored configurations are categorized as accurate. The details of our training setups can be found in the supporting information (Text S1 and Figure. S1).

The accuracy of the deep-learning potential was firstly confirmed by comparing the predicted energy, forces, and pressures with those from the first-principles approach (Figure. S2 and Figure. S3). Mean-square displacements and radial distribution functions calculated by the deep-learning potential were also shown to be comparable with the corresponding first-principles results (Figure. S4). These results also confirmed that the simulated systems are in the liquid state over the pressure-temperature range considered in this study. The viscosity was calculated by using the Green-Kubo relation

$$\eta = \frac{V}{k_{\mathrm{B}}T} \int_0^{\infty} \langle \tau_{\alpha\beta}(t + t_0) \cdot \tau_{\alpha\beta}(t_0) \rangle \, dt, \quad (1)$$

where V is volume, k_B is the Boltzmann constant, T is the temperature, $\tau_{\alpha\beta}$ is the stress tensor, t is time, and t_0 is the time origin. The ionic electrical conductivity was calculated by using the following equation (e.g., Ghosh & Karki, 2017; Müller-Plathe, 1994)

$$\sigma = \frac{1}{k_B TV} lim_{t\to\infty} \frac{1}{6t} \langle \left| \sum_{i=1}^{N} z_i (\vec{r}_i(t + t_0) - \vec{r}_i(t_0)) \right|^2 \rangle, \quad (2)$$

where z_i is the Bader charge, $\vec{r}(t)$ denotes the atomic trajectories and $\langle ... \rangle$ represents an average at time t from different time origins t_0. This equation is based on modified Einstein relation after adding the charge of species. The Green-Kubo relation for ionic conductivity is not used here because it requires a high frequency of velocity information saving to guarantee the accuracy of integration in practice. Theoretically, the two relations are equivalent. Equation (2) should be more robust than the indirect approach of estimating electrical conductivity from the self-diffusivities of n_a species via the Nernst-Einstein equation: $\sigma_{NE} = \frac{1}{k_B T} \sum_{i=1}^{n_a} \rho_i z_i^2 D_i$, where ρ_i is the number density of species i with charge z_i and diffusivity D_i. The Nernst-Einstein equation fails to consider the correlation of ionic motions, which could be important in silicate melts. We checked the finite-size effect on the viscosity, electrical conductivity, and self-diffusivity using four systems of different sizes up to 640 atoms (Figure. S5). The viscosity and electrical conductivity were found to be insensitive to the system size. The self-diffusivity was found to increase with increasing system size as an approximately linear function of $N^{-1/3}$ (where N is the number of atoms), consistent with the correction relation proposed by Yeh and Hummer (2004) so we applied the correction to the diffusivity accordingly.

3 Results and Discussion

3.1 Viscosity of $MgSiO_3$ melt

We find the viscosity increases with increasing pressure above ~6 GPa along all isotherms, but the pressure dependence of the viscosity at lower pressures gradually changes from positive to negative with decreasing temperature (Figure. 1a). For example, at relatively low temperatures (<3000 K), the viscosity initially decreases with increasing pressure and then starts increasing after a minimum value is reached. The pressure corresponding to the viscosity turnover is ~6 GPa at 2200 K, which is close to the pressure range found in polymerized silicate melts (e.g., Sakamaki et al., 2013; Suzuki et al., 2011). Our results above 3000 K are broadly consistent with those from first-principles simulations (Karki & Stixrude, 2010), and the variation of the viscosity with temperature and pressure is more self-consistent (Figure. 1a) because of ~5 orders of magnitude larger statistics. The predicted values and anomalous decrease of the viscosity around 2100-2200 K are consistent with the results of experimental studies at pressures below ~8 GPa (Cochain et al., 2017; Xie et al., 2020). However, three of the viscosity data reported by the experiments (Xie et al., 2020) at 2623 K and 15.3 GPa, 2836 K and 24.1 GPa, and 3250 K and 29.9 GPa are only about half of our calculated values. It is not clear what causes the discrepancy.

We also find that the viscosity is tied to the slow-diffusing Si and O, whose diffusivities show an almost exactly opposite relationship with temperature and pressure (Figure. 2) compared to that of the viscosity (the viscosity-diffusivity relation in a quantitative sense is further discussed in Figure S6). The viscosity and diffusivity turnover can be attributed to the tetrahedral packing limit (Wang et al., 2014). At relatively low temperatures (<3000 K), the initial effect of pressure on increasing bridging oxygen (BO, oxygen atoms that are shared by network formers such as Si here) at the expense of non-bridging oxygen (NBO, oxygen atoms bonded to only one network former) is attenuated (Figure. 1b) due to the decreasing voids and consequently the reduced size of the diffusing units, which lead to a decrease in the viscosity and

an increase in the diffusivities of Si and O. The pentahedral coordination species acts as transition state for diffusion because when NBO ←→ BO and SiO_4 ←→ SiO_5 reactions take place, one oxygen (NBO) enters the coordination shell and some other oxygen (BO) may leave the coordination shell. Once the packing limit is reached, further packing with increasing pressure results in a rapid increase in BO at the expense of NBO (Figure. 1b) (and consistently enhanced abundances of high-coordination species, including SiO_5 and SiO_6), which favors structural polymerization and lead to an increase in the viscosity and a decrease in the diffusivity. At high temperatures (>3500 K), further packing rather than a weak structure rearrangement (changes in the medium range order, owing to high flexibility and polyhedral distortion caused by increased kinetic energy) is favored even starting from zero pressure, as evidenced by the rapid decrease of NBO (Figure. 1b). Thus, the viscosity increases continuously with increasing pressure as normally expected.

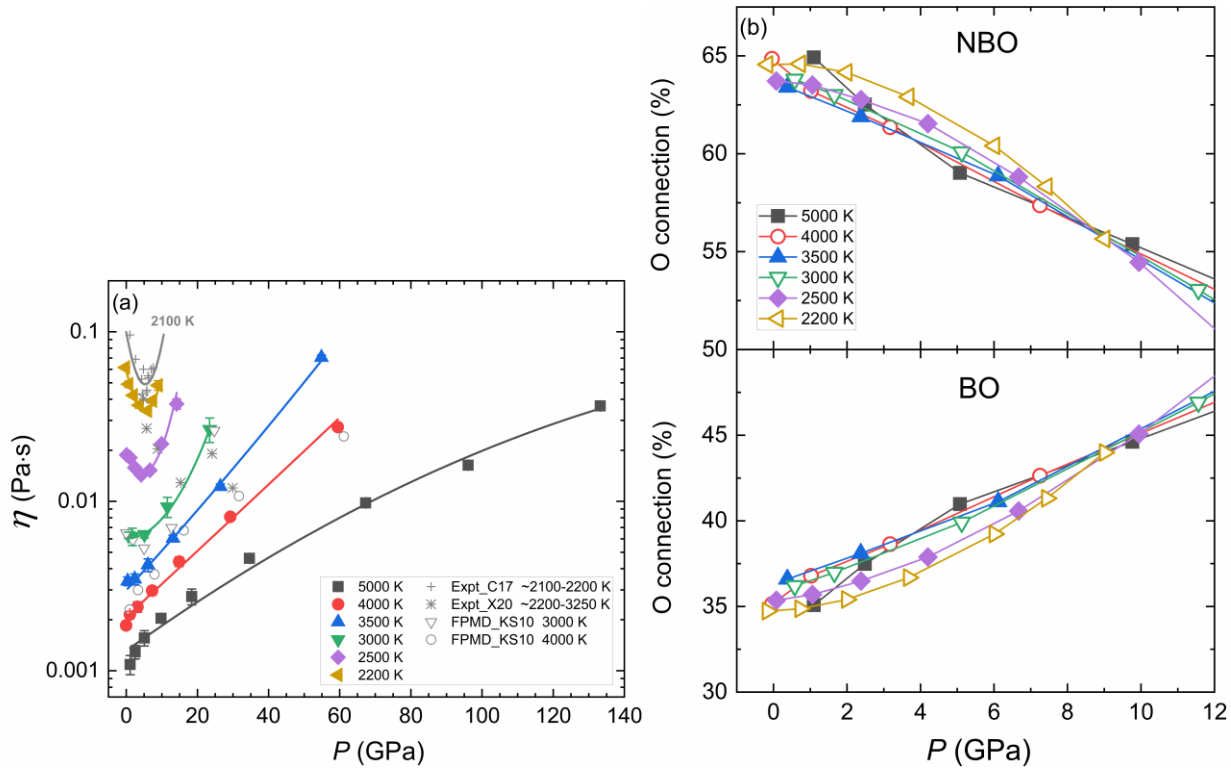

Figure 1. (a) Calculated viscosity (η) of $MgSiO_3$ melt at different temperatures as a function of pressure compared with previous first-principles results (Karki & Stixrude, 2010). Our results can be represented by the modified VFT (Vogel-Fulcher-Tammann) equation (Harris et al., 2005) within two temperature ranges, $\eta(P,T) = \exp[-8.53 + 0.325\,P - 0.0247\,P^2 + (6851 - 651\,P + 54.8\,P^2)/(T - 1000)]$ with $2200 \leq T \leq 3000$ K; and $\eta(P,T) = \exp[-8.00 + 0.00377\,P - 0.000315\,P^2 + (5470 + 123\,P + 0.963\,P^2)/(T - 1000)]$, with $3500 \leq T \leq 5000$ K. The experimental data (Cochain et al., 2017; Xie et al., 2020) are compared with the predicted viscosity along 2100 K using the VFT model. (b) The proportion of non-bridging oxygen (NBO) and bridging oxygen (BO) in $MgSiO_3$ melt at different temperatures as a function of pressure up to 12 GPa. Note that free oxygen present in small amount is also counted in NBO. BO includes oxygen connecting two or more silicon atoms.

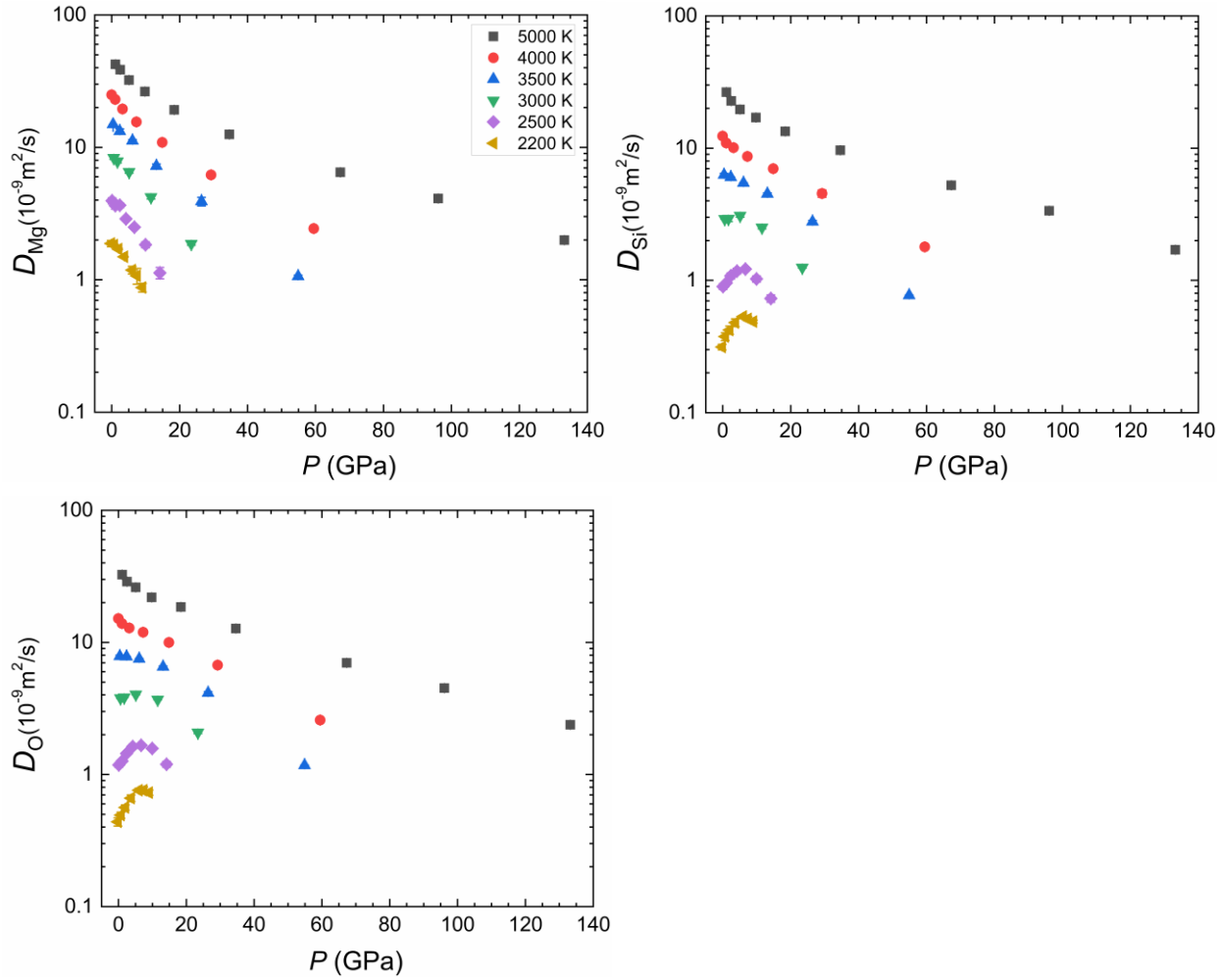

Figure 2. Calculated diffusivities of Mg, Si, and O at different temperatures and pressures.

3.2 Electrical conductivity of $MgSiO_3$ melt

The electrical conductivity appears to first increase, then decrease with increasing pressure at all temperatures (Figure. 3a), although the decreasing trend is not so clear at 2200 K. Furthermore, the pressure corresponding to the electrical conductivity turnover decreases with decreasing temperature (Figure. 3a). Our results at 4000 and 5000 K are broadly consistent with those from previous first-principles simulations (Ghosh & Karki, 2017). However, our predicted electrical conductivities at 1873 K are higher than experimental results in dry basaltic melts. Also, previous experiments found the electrical conductivity decreasing with pressure at below 3 GPa in natural silicate melts (e.g., Laumonier et al., 2015; Ni et al., 2011; Tyburczy & Waff, 1983). These differences can be attributed to the existence of Na in experiments, which is the dominant charge carrier due to its fast diffusion (e.g., Gaillard, 2004; Ni et al., 2011).

Diffusion and correlated motion of ions play competitive roles in determining electrical conductivity. Higher diffusion rates of ions generally mean higher electrical conductivity, but more correlated motions of ions result in lower electrical conductivity because of possible charge cancellation. We find that even though all the diffusivities of Mg, Si, and O decrease with increasing pressure at relatively high temperatures (>3500 K) (Figure. 2), the electrical

conductivity still increases at first, suggesting that the correlation of ionic motions plays a crucial role here. The correlation of ionic motions can be estimated by the ratio of calculated electrical conductivity by the Nernst-Einstein equation to the direct results (σ_{NE}/σ). The smaller and the closer to the unity the ratio is, the less correlated ionic motions are (that is, the more effective cation-anion dissociation is). The initial increase in the electrical conductivity at relatively high temperatures (>3500 K) makes sense because of the decreasing correlation of ionic motions (Figure. 3b). As temperature decreases and pressure increases, cation-anion dissociation tends to become more effective, so the ions diffuse more independent of each other. However, the initial increase in the electrical conductivity at lower temperatures (<3000 K) is contrary to the effect of increasing correlation of ionic motions (Figure. 3), implying that the increasing diffusivities of Si and O (Figure. 2) overwhelms the effect of more correlated ionic motions at low pressures. Furthermore, we find that the correlation parameter (σ_{NE}/σ) is negatively associated with the viscosity. The more viscous the melt is, the less correlated ionic motions are.

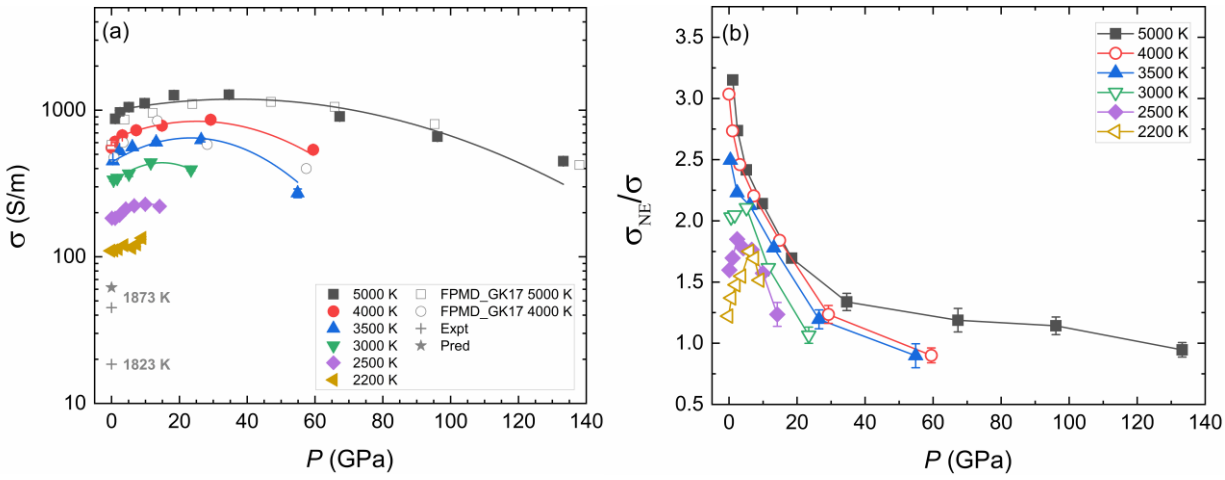

Figure 3. (a) Calculated electrical conductivity (σ) of $MgSiO_3$ melt at different temperatures as a function of pressure compared with previous first-principles simulations (Ghosh & Karki, 2017). Our results can be represented by the modified VFT (Vogel-Fulcher-Tammann) equation (Harris et al., 2005) within two temperature ranges:
$\sigma(P,T) = \exp[7.44 + 0.0443\,P + 0.000117\,P^2 + (-3353 - 3.92\,P - 3.08\,P^2)/(T - 1000)]$ with $2200 \leq T \leq 3000$ K; and
$\sigma(P,T) = \exp[8.23 - 0.0268\,P + 0.000786\,P^2 + (-5343 + 149\,P - 3.72\,P^2)/(T - 1000)]$, with $3500 \leq T \leq 5000$ K. The experimental data (pluses) at 1823 and 1873 K for dry basaltic melts (Presnall et al., 1972; Waff & Weill, 1975) are compared with the predicted result at 1873 K (star) using the VFT equation. (b) The ratio of calculated electrical conductivity by Nernst-Einstein equation (σ_{NE}) to our direct results at different temperatures as a function of pressure. The errors are shown for the selected results for the sake of clarity.

4 Implications

Based on the new viscosity results at lower temperatures, we evaluate the viscosity profiles of $MgSiO_3$ melt along mantle liquidus and magma ocean isentropes (Mosenfelder et al., 2009; Stixrude et al., 2009) (Figure. 4a). The one along mantle solidus would take the same shape as that along mantle liquidus with a systematic shift upward (Karki & Stixrude, 2010). An initial decrease in the viscosity profiles with pressure up to ~7 GPa implies that a shallower

magma ocean (or a magma pond) would cool faster than previously thought provided the same thermally conductive lid, as the cooling rate of magma ocean is inversely correlated with its viscosity (Monteux et al., 2016). It also implies that silicate melts in the present-day Earth's asthenosphere would tend to accumulate in the lithosphere-asthenosphere boundary as suggested by the experiments on basaltic melt (Sakamaki et al., 2013). We also find a viscosity turnover along mantle liquidus at ~23 GPa (Figure. 4a) corresponding to the 660 km discontinuity between the transition zone and lower mantle. The melt zone model suggests that melt fraction at depth negatively correlates with the ratio of melt-solid density contrast ($\Delta\rho$) to the melt viscosity (η) (Schubert et al., 2001). The abundance of volatile elements (e.g., H, C) can influence the melt viscosity but usually results in a systematic shift upward (Karki & Stixrude, 2010). Thus, the predicted viscosity maximum at ~23 GPa could lead to a melt accumulation near the top of the lower mantle, which explains the observed abrupt seismic velocity decreases there. Note that the viscosity turnover here is based on a mantle liquidus curve and extrapolated calculation of our viscosity results. Studies on melts with more realistic compositions in a wider temperature-pressure range may help to check the turnover.

The electrical conductivity of $MgSiO_3$ melt along mantle liquidus first increases up to ~420 S/m at ~50 GPa and then decreases to ~26 S/m at the core-mantle boundary (CMB, ~135 GPa) (Figure. 4b). Minor melt distribution combined with the rapid rise in the electrical conductivity of melt may contribute to the steep increase of the electrical conductivity profiles in the upper part of the lower mantle derived from magnetic field measurements (Püthe et al., 2015). The considerably large value of the melt electrical conductivity at the CMB (Figure. 4b) with further possible enhancement by dissolved volatile elements suggests the potential use of magnetotelluric observations in constraining the presence of melt in the Earth's deep mantle (e.g., ultralow-velocity zones). When melt and solid conductivities are known, the melt fraction can be estimated based on Hashin-Shtrikman bounds (Hashin & Shtrikman, 1962) on the bulk conductivity of the mantle ($\sigma_{HS+}$and σ_{HS-}) expressed as

$$\sigma_{HS\pm} = \left[\frac{\phi}{\sigma_m+2\sigma_{m/s}} + \frac{1-\phi}{\sigma_s+2\sigma_{m/s}}\right]^{-1} - 2\sigma_{m/s} \quad (3)$$

where ϕ is the melt fraction, σ_m and σ_s are the conductivity of melt and solid, $\sigma_{m/s}$ is the conductivity of melt (in the case of σ_{HS+}) or solid (in the case of σ_{HS-}). Our estimated melt fraction is ~1.7-6.8 % given a solid electrical conductivity value of 2 S/m at the core-mantle boundary (Figure. 4b). Here we have only considered ionic contributions to electrical conductivity calculated from our deep potential molecular dynamics simulations, which accurately describe ionic motions without dealing with electronic structure. It has been recently suggested that electronic conductivities of silicate melts could exceed 10,000 S/m at the CMB and thus dominate ionic conductivities (Soubiran & Militzer, 2018; Stixrude et al., 2020). Based on such high electrical conductivity, the estimated melt fraction would be much smaller (~ 0.005-5.7 %).

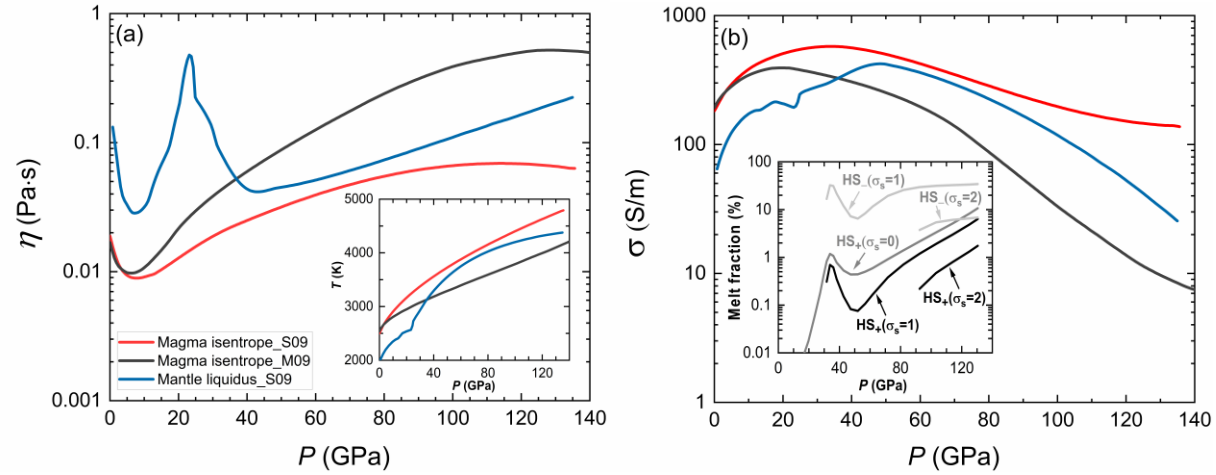

Figure 4. (a) Predicted viscosity and (b) electrical conductivity profiles along magma ocean isentropes (Mosenfelder et al., 2009; Stixrude et al., 2009) and mantle liquidus (Stixrude et al., 2009) shown in the inset of (a) using the modified VFT equations. Predicted viscosity and electrical conductivity values in the temperature range of 3000 to 3500 K are obtained by Akima spline interpolation method. The inset in (b) shows an estimation of melt fraction based on the melt electrical conductivity profile along the mantle liquidus given a constant value of solid electrical conductivity (0, 1, and 2 S/m) using the Earth's radial conductivity structure from Püthe et al. (2015).

Acknowledgments

This work is supported by the Strategic Priority Research Program (B) of Chinese Academy of Sciences (XDB18010104) and National Science Foundation (EAR 1764140 and 2001074). High-performance computing resources were provided by Louisiana State University.

Data Availability Statement

Dataset used in this study has been deposited at the Open Science Framework (https://osf.io/xm3gq/) with DOI: 10.17605/OSF.IO/XM3GQ.

References

Blochl, P. E. (1994). Projector Augmented-Wave Method. *Physical Review B, 50*(24), 17953-17979. doi:https://doi.org/10.1103/PhysRevB.50.17953

Canup, R. M. (2004). Simulations of a late lunar-forming impact. *Icarus, 168*(2), 433-456. doi:https://doi.org/10.1016/j.icarus.2003.09.028

Ceperley, D. M., & Alder, B. J. (1980). Ground-State of the Electron-Gas by a Stochastic Method. *Physical Review Letters, 45*(7), 566-569. doi:https://doi.org/10.1103/PhysRevLett.45.566

Cochain, B., Sanloup, C., Leroy, C., & Kono, Y. (2017). Viscosity of mafic magmas at high pressures. *Geophysical Research Letters, 44*(2), 818-826. doi:https://doi.org/10.1002/2016GL071600

Elkins-Tanton, L. T. (2012). Magma Oceans in the Inner Solar System. *Annual Review of Earth and Planetary Sciences, 40*(1), 113-139. doi:10.1146/annurev-earth-042711-105503

Gaillard, F. (2004). Laboratory measurements of electrical conductivity of hydrous and dry silicic melts under pressure. *Earth and Planetary Science Letters, 218*(1), 215-228. doi:https://doi.org/10.1016/S0012-821X(03)00639-3

Ghosh, D. B., & Karki, B. B. (2017). Transport properties of carbonated silicate melt at high pressure. *Science Advances, 3*(12), e1701840. doi:10.1126/sciadv.1701840

Harris, K. R., Woolf, L. A., & Kanakubo, M. (2005). Temperature and Pressure Dependence of the Viscosity of the Ionic Liquid 1-Butyl-3-methylimidazolium Hexafluorophosphate. *Journal of Chemical & Engineering Data, 50*(5), 1777-1782. doi:10.1021/je050147b

Hashin, Z., & Shtrikman, S. (1962). A Variational Approach to the Theory of the Effective Magnetic Permeability of Multiphase Materials. *Journal of Applied Physics, 33*(10), 3125-3131. doi:10.1063/1.1728579

Karki, B. B., & Stixrude, L. P. (2010). Viscosity of $MgSiO_3$ Liquid at Earth's Mantle Conditions: Implications for an Early Magma Ocean. *Science, 328*(5979), 740-742. doi:10.1126/science.1188327

Kresse, G., & Furthmuller, J. (1996). Efficiency of ab-initio total energy calculations for metals and semiconductors using a plane-wave basis set. *Computational Materials Science, 6*(1), 15-50. doi:Doi 10.1016/0927-0256(96)00008-0

Kresse, G., & Joubert, D. (1999). From ultrasoft pseudopotentials to the projector augmented-wave method. *Physical Review B, 59*(3), 1758-1775. doi:https://doi.org/10.1103/PhysRevB.59.1758

Lange, R. A., & Carmichael, I. S. E. (1987). Densities of Na2O-K2O-CaO-MgO-FeO-Fe2O3-Al2O3-TiO2-SiO2 liquids: New measurements and derived partial molar properties. *Geochimica Et Cosmochimica Acta, 51*(11), 2931-2946. doi:https://doi.org/10.1016/0016-7037(87)90368-1

Laumonier, M., Gaillard, F., & Sifré, D. (2015). The effect of pressure and water concentration on the electrical conductivity of dacitic melts: Implication for magnetotelluric imaging in subduction areas. *Chemical Geology, 418*, 66-76. doi:10.1016/j.chemgeo.2014.09.019

Liebske, C., Schmickler, B., Terasaki, H., Poe, B. T., Suzuki, A., Funakoshi, K.-i., . . . Rubie, D. C. (2005). Viscosity of peridotite liquid up to 13 GPa: Implications for magma ocean viscosities. *Earth and Planetary Science Letters, 240*(3), 589-604. doi:https://doi.org/10.1016/j.epsl.2005.10.004

Monteux, J., Andrault, D., & Samuel, H. (2016). On the cooling of a deep terrestrial magma ocean. *Earth and Planetary Science Letters, 448*, 140-149. doi:https://doi.org/10.1016/j.epsl.2016.05.010

Mosenfelder, J. L., Asimow, P. D., Frost, D. J., Rubie, D. C., & Ahrens, T. J. (2009). The MgSiO3 system at high pressure: Thermodynamic properties of perovskite, postperovskite, and melt from global inversion of shock and static compression data. *Journal of Geophysical Research: Solid Earth, 114*(B1). doi:https://doi.org/10.1029/2008JB005900

Müller-Plathe, F. (1994). Permeation of polymers — a computational approach. *Acta Polymerica, 45*(4), 259-293. doi:https://doi.org/10.1002/actp.1994.010450401

Ni, H., Hui, H., & Steinle-Neumann, G. (2015). Transport properties of silicate melts. *Reviews of Geophysics, 53*(3), 715-744. doi:https://doi.org/10.1002/2015RG000485

Ni, H., Keppler, H., Manthilake, M. A. G. M., & Katsura, T. (2011). Electrical conductivity of dry and hydrous $NaAlSi_3O_8$ glasses and liquids at high pressures. *Contributions to Mineralogy and Petrology, 162*, 501. doi:10.1007/s00410-011-0608-5

Plimpton, S. (1995). Fast parallel algorithms for short-range molecular-dynamics. *Journal of Computational Physics, 117*(1), 1-19. doi:10.1006/jcph.1995.1039

Presnall, D. C., Simmons, C. L., & Porath, H. (1972). Changes in electrical conductivity of a synthetic basalt during melting. *Journal of Geophysical Research (1896-1977), 77*(29), 5665-5672. doi:https://doi.org/10.1029/JB077i029p05665

Püthe, C., Kuvshinov, A., Khan, A., & Olsen, N. (2015). A new model of Earth's radial conductivity structure derived from over 10 yr of satellite and observatory magnetic data. *Geophysical Journal International, 203*(3), 1864-1872. doi:10.1093/gji/ggv407

Reid, J. E., Suzuki, A., Funakoshi, K.-I., Terasaki, H., Poe, B. T., Rubie, D. C., & Ohtani, E. (2003). The viscosity of CaMgSi2O6 liquid at pressures up to 13GPa. *Physics of the Earth and Planetary Interiors, 139*(1), 45-54. doi:https://doi.org/10.1016/S0031-9201(03)00143-2

Sakamaki, T., Suzuki, A., Ohtani, E., Terasaki, H., Urakawa, S., Katayama, Y., . . . Ballmer, M. D. (2013). Ponded melt at the boundary between the lithosphere and asthenosphere. *Nature Geoscience, 6*(12), 1041-1044. doi:10.1038/ngeo1982

Schubert, G., Turcotte &, D. L., & Olson, P. (2001). Mantle Convection in the Earth and Planets 940. *Cambridge University Press*.

Solomatova, V. S. (2007). Magma oceans and primordial mantle differentiation. *In Treatise on Geophysics, Vol. 9: Evolution of the Earth, ed. DJ Stevenson, pp. 91–119. Amsterdam: Elsevier*, 9, 91–120.

Soubiran, F., & Militzer, B. (2018). Electrical conductivity and magnetic dynamos in magma oceans of Super-Earths. *Nature Communications, 9*(1), 3883. doi:10.1038/s41467-018-06432-6

Spice, H., Sanloup, C., Cochain, B., de Grouchy, C., & Kono, Y. (2015). Viscosity of liquid fayalite up to 9GPa. *Geochimica Et Cosmochimica Acta, 148*, 219-227. doi:https://doi.org/10.1016/j.gca.2014.09.022

Stixrude, L., de Koker, N., Sun, N., Mookherjee, M., & Karki, B. B. (2009). Thermodynamics of silicate liquids in the deep Earth. *Earth and Planetary Science Letters, 278*(3), 226-232. doi:https://doi.org/10.1016/j.epsl.2008.12.006

Stixrude, L., Scipioni, R., & Desjarlais, M. P. (2020). A silicate dynamo in the early Earth. *Nature Communications, 11*(1), 935. doi:10.1038/s41467-020-14773-4

Suzuki, A., Ohtani, E., Terasaki, H., Nishida, K., Hayashi, H., Sakamaki, T., . . . Kikegawa, T. (2011). Pressure and temperature dependence of the viscosity of a NaAlSi2O6 melt. *Physics and Chemistry of Minerals, 38*(1), 59-64. doi:10.1007/s00269-010-0381-4

Tyburczy, J. A., & Waff, H. S. (1983). Electrical conductivity of molten basalt and andesite to 25 kilobars pressure: Geophysical significance and implications for charge transport and melt structure. *Journal of Geophysical Research: Solid Earth, 88*(B3), 2413-2430. doi:https://doi.org/10.1029/JB088iB03p02413

Verma, A. K., & Karki, B. B. (2012). First-principles study of self-diffusion and viscous flow in diopside (CaMgSi2O6) liquid. *American Mineralogist, 97*(11-12), 2049-2055. doi:10.2138/am.2012.4123

Waff, H. S., & Weill, D. F. (1975). Electrical conductivity of magmatic liquids: effects of temperature, oxygen fugacity and composition. *Earth and Planetary Science Letters, 28*(2), 254-260. doi:https://doi.org/10.1016/0012-821X(75)90235-6

Wang, H., Zhang, L. F., Han, J. Q., & E, W. N. (2018). DeePMD-kit: A deep learning package for many-body potential energy representation and molecular dynamics. *Computer Physics Communications, 228*, 178-184. doi:10.1016/j.cpc.2018.03.016

Wang, Y., Sakamaki, T., Skinner, L. B., Jing, Z., Yu, T., Kono, Y., . . . Sutton, S. R. (2014). Atomistic insight into viscosity and density of silicate melts under pressure. *Nature Communications, 5*(1), 3241. doi:10.1038/ncomms4241

Xie, L., Yoneda, A., Yamazaki, D., Manthilake, G., Higo, Y., Tange, Y., . . . Andrault, D. (2020). Formation of bridgmanite-enriched layer at the top lower-mantle during magma ocean solidification. *Nature Communications, 11*(1), 548. doi:10.1038/s41467-019-14071-8

Yeh, I.-C., & Hummer, G. (2004). System-Size Dependence of Diffusion Coefficients and Viscosities from Molecular Dynamics Simulations with Periodic Boundary Conditions. *The Journal of Physical Chemistry B, 108*(40), 15873-15879. doi:10.1021/jp0477147

Zhang, L. F., Han, J. Q., Wang, H., Car, R., & Weinan, E. (2018a). Deep Potential Molecular Dynamics: A Scalable Model with the Accuracy of Quantum Mechanics. *Physical Review Letters, 120*(14). doi:10.1103/PhysRevLett.120.143001

Zhang, L. F., Han, J. Q., Wang, H., Saidi, W., Car, R., & Weinan, E. (2018b). End-toend symmetry preserving inter-atomic potential energy model for finite and extended systems. *Advances of the Neural Information Processing Systems*.

Zhang, Y. Z., Wang, H. D., Chen, W. J., Zeng, J. Z., Zhang, L. F., Wang, H., & Weinan, E. (2020). DP-GEN: A concurrent learning platform for the generation of reliable deep learning based potential energy models. *Computer Physics Communications, 253*. doi:10.1016/j.cpc.2020.107206